W-Band ^{17}O Pulsed Electron Nuclear Double Resonance Study of Gadolinium Complexes with Water

Arnold M. Raitsimring* and Andrei V. Astashkin*

Department of Chemistry, University of Arizona, Tucson, Arizona 85721

Debbie Baute and Daniela Goldfarb

The Weizmann Institute of Science, Rehovot 76100, Israel

Peter Caravan

EPIX Medical, Inc., 71 Rogers Street, Cambridge, Massachusetts 02142

Received: April 22, 2004; In Final Form: June 21, 2004

In this work we have studied pulsed ^{17}O electron nuclear double resonance (ENDOR) spectra of the Gd^{3+} aquo ion and the magnetic resonance imaging (MRI) contrast agent MS-325 in an ^{17}O-enriched frozen glassy water/methanol solution. The isotropic hyperfine interaction (hfi) constant of the water ligand ^{17}O was found to be about 0.75 MHz, which corresponds to a spin density delocalized to the ligand of $\rho_O \approx -4 \times 10^{-3}$. The analysis of the anisotropic hfi constant (0.69 ± 0.05 MHz) yields Gd−O distances of about 2.4−2.5 Å. Simultaneous analysis of these distances and the Gd−H distances found earlier allows one to elucidate the details of the $Gd-OH_2$ coordination geometry.

Introduction

The interaction of metal ions with water molecules is an area of active exploration for both fundamental and applied reasons. In particular, the interaction of water with the Gd^{3+} ion is central to the use of gadolinium complexes as contrast agents in magnetic resonance imaging (MRI).[1−4] The gadolinium ion acts as a magnetic catalyst to shorten the relaxation times of protons of water molecules that it comes into contact with. The relaxation mechanism is dipolar, and its efficiency critically depends on the complex structure, in particular, on the Gd−proton distance, R_{GdH}. It is therefore clear that the knowledge of geometrical structures of Gd^{3+} complexes is important for understanding and predicting the efficiency of this relaxation enhancement. It may also reveal correlations between the structure and dynamic properties such as the exchange rate of water ligands. Ultimately, the knowledge of the complex structures in solution serves as a starting point for development of improved prospective MRI contrast agents.

With few exceptions, information on the geometry of lanthanide complexes was obtained by X-ray crystallography,[5,6] neutron diffraction,[7,8] and extended X-ray absorption fine structure (EXAFS).[9] The usefulness of this information for predicting the relaxation properties of the Gd complexes, however, depends on our understanding of the relationship between the structure and the dipole interactions of water ligand protons. It is well established that this relationship may generally be significantly more complex than that described by a simple point dipole model because some spin density is transferred from the central ion to the oxygen of the ligand water molecule.[10−14] This delocalized spin density, ρ_O, can be evaluated from the ^{17}O hyperfine interactions (hfi) obtained by various magnetic resonance techniques. The estimates currently available in the literature represent the average values obtained by ^{17}O nuclear magnetic resonance (NMR) in liquid solutions.[11] To our knowledge, there are no data in the literature on ^{17}O hfi in Gd^{3+} complexes stabilized in frozen glassy solutions where all possible complex configurations are realized.

The magnetic resonance techniques best suited for measuring weak hfi of various nuclei in paramagnetic centers in frozen glassy solutions are those of electron nuclear double resonance (ENDOR) and electron spin−echo envelope modulation (ESEEM). In particular, these techniques have a long record of successful investigations of the nearby nuclear environments of metal centers, including both the qualitative identification of ligands and the quantitative structural information obtained from analysis of the hfi and nuclear quadrupole interactions (nqi).[15]

In our earlier ^1H pulsed ENDOR study of Gd^{3+} complexes[16] we determined the hf interactions of the protons of water ligands. The Gd−H distances, R_{GdH}, were then estimated using a simple point dipole approximation and neglecting any possible effects of the spin density delocalized to the ligand oxygen. The justification of this approach was based on indirect evidence that included the weakness of the ^1H isotropic hfi,[16] the ^{17}O NMR results,[10−14] and ^{19}F ENDOR data for lanthanide complexes in single crystals.[17] In this work, to put the structural analysis of the proton hfi data on more solid ground, we performed a pulsed ENDOR study of Gd^{3+} complexes with $H_2{}^{17}O$.

The ^{17}O pulsed ENDOR spectra of frozen glassy solutions of two Gd^{3+} complexes were recorded and analyzed in order to evaluate the hf and nq interactions of the ligand ^{17}O. The ^{17}O hfi parameters determined from these spectra yielded information about the Gd−O(water) distance in the complexes

* To whom correspondence should be addressed. For A.M.R.: phone, (520) 621-9968; fax, (520) 621-8407; e-mail, arnold@u.arizona.edu. For A.V.A.: phone, (520) 621-9968; fax, (520) 621-8407; e-mail: andrei@u.arizona.edu.

10.1021/jp040306i CCC: $27.50
Published on Web 08/06/2004

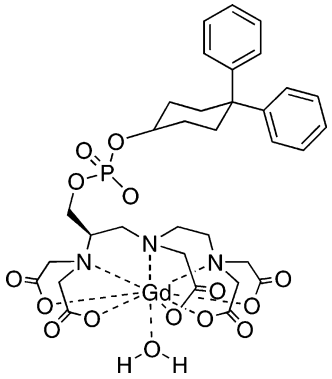

Figure 1. Structure of the MRI contrast agent MS-325.

and about the spin delocalization on the oxygen ligand. This study has confirmed that the spin density transfer to the oxygen ligand can indeed be ignored when interpreting the anisotropic hfi of the water ligand protons, as was proposed previously.[16] Moreover, the spin density on the water oxygen ligand is sufficiently small to be safely neglected when estimating the Gd−O distance from the ^{17}O anisotropic hfi.

One of the major issues in our previous K_u-band ^1H pulsed ENDOR work[16] was to account for the ENDOR spectral manifestations of the crystal field interactions (cfi) of the Gd^{3+} electron spin $S = 7/2$. In this work, following earlier examples,[18,19] we used a considerably higher microwave (mw) frequency of ∼95 GHz (W-band) and, correspondingly, higher magnetic field ($B_o \approx 3.4$ T), which resulted in the ENDOR spectra being virtually free from the cfi-related effects.

Experimental Section

The ^{17}O-enriched (70%) H_2O was purchased from Cambridge Isotope Laboratories, Inc. The experiments were performed with frozen 1 mM solutions of Gd^{3+} aquo complex (prepared by dissolving $GdCl_3 \cdot 6H_2O$) or MS-325 contrast agent (Epix Medical; see Figure 1) in 1:1 (v/v) H_2O/CH_3OH (methanol added for glassification). The pH of the water was about 5. It is unlikely that there will be any hydroxo species present under these conditions. The first pK_a of the gadolinium aquo ion is ∼8.[20] Dissolution of $GdCl_3$ into pH 5 water should not result in appreciable amounts of the hydroxogadolinium species. For MS-325, it was shown[21] that over the pH range 3−11 there is only one species present, that shown in Figure 1. There was no evidence of a hydroxo species; that is, the pK_a of the coordinated water was >11. Details on the size and handling of the samples can be found elsewhere.[22] The experiments were performed on a W-band (∼95 GHz) pulsed EPR spectrometer[22] using Mims ENDOR technique.[23] The measurement temperature was about 5.3 K.

Results and Discussion

1. Electron Spin Echo (ESE) Field Sweeps. Figure 2 shows the field-sweep spectra of the Gd^{3+} aquo and MS-325 complexes detected using the primary ESE technique. The central intense peak in these spectra located at the magnetic field $B_o \approx 3.3966$ T represents the line of the $-1/2 \leftrightarrow +1/2$ transition of the Gd^{3+} electron spin $S = 7/2$, while the broad featureless background is contributed by all other transitions. The ENDOR measurements were performed at B_o corresponding to positions A (3.3966 T) and B (3.4060 T) in the field sweep spectra. It is important to note that at position A the contribution of the $-1/2 \leftrightarrow +1/2$ transition to the amplitude of the ESE signal is about 75% while all other transitions contribute the remaining ∼25%.

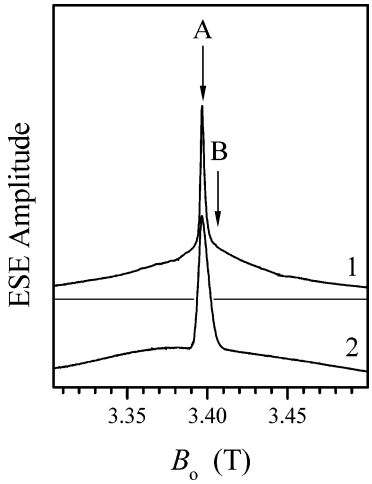

Figure 2. Field sweep spectra of Gd complexes detected using primary ESE technique. Traces 1 and 2 correspond to Gd aquo and MS-325, respectively. Positions marked A and B are those where the ENDOR experiments were performed. Experimental conditions are the following: mw frequency, 94.9 GHz; durations of the mw pulses, 60 ns; time interval τ between the pulses, 300 ns.

2. Mims ENDOR Spectra of ^{17}O. Solid trace A and trace B in Figure 3 show normalized (by stimulated ESE amplitude) ^{17}O Mims ENDOR spectra of the Gd^{3+} aquo ion recorded at EPR positions A and B (see Figure 2), respectively. Analysis of these spectra must take into account that while spectrum A has contributions from all possible EPR transitions, the EPR transition $-1/2 \leftrightarrow +1/2$ does not contribute to spectrum B. The magnetic field difference of ∼9.4 mT between the EPR positions A and B is considerably smaller than the characteristic value of the cfi parameter D (for the aquo complex, $D/(g\beta) \approx 30$ mT[24,25]), and therefore, the ENDOR spectra arising from all EPR transitions other than the $-1/2 \leftrightarrow +1/2$ one at positions A and B should be practically identical. This enables us to obtain the ENDOR spectrum arising solely from the EPR transition $-1/2 \leftrightarrow +1/2$ by subtracting spectrum B from spectrum A after adjusting their relative amplitudes. The adjusted ENDOR spectrum B is shown by dashed trace A superimposed on solid trace A in Figure 3. One can see that the contribution of spectrum B to solid trace A is very small and is mainly evident as a weak shoulder at the low-frequency side of solid trace A. Trace A-B in Figure 3 represents the difference spectrum that shows the nuclear transitions within the $m_S = \pm 1/2$ electron spin manifolds only.

Apart from the central broad feature that may be, at least in part, attributed to distant matrix oxygens, the difference spectrum may be described as consisting of two narrow peaks with a splitting of ∼1.33 MHz between them and two sets of shoulders with splittings of about 3.3 and 5.1 MHz. To understand this spectral shape, the theoretical and experimental background will first be discussed, followed by numerical simulations to obtain the interaction parameters for the ^{17}O nuclei of the water ligands.

The ^{17}O nucleus has spin $I = 5/2$ and a nonzero nqi. The spin Hamiltonian accounting for the ^{17}O Zeeman interaction, hfi, and nqi can be written as follows:

$$\hat{H} = -\nu_O \hat{I}_Z + m_S[T_{ZX}\hat{I}_X + T_{ZY}\hat{I}_Y + (a_{iso} + T_{ZZ})\hat{I}_Z] + k[3\hat{I}_{Z'}^2 + \eta(\hat{I}_{X'}^2 - \hat{I}_{Y'}^2)] \quad (1)$$

where ν_O is the Zeeman frequency of ^{17}O, a_{iso} is the isotropic hfi constant, T_{Zj} ($j = X, Y, Z$) are the relevant components of

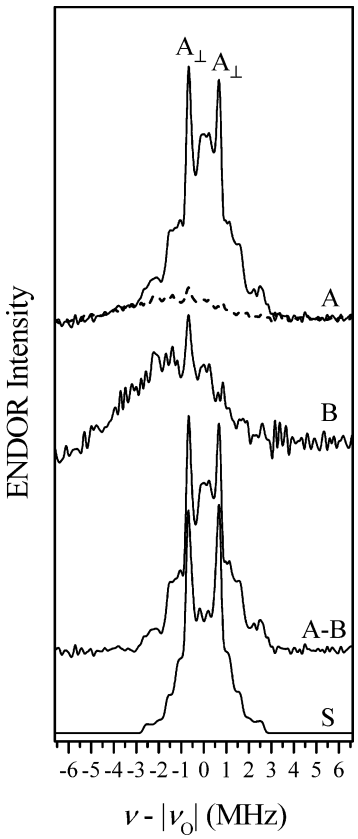

Figure 3. Solid traces A and B are the ^{17}O Mims ENDOR spectra of Gd aquo complex recorded at $B_o = 3.3966$ T (point A; see Figure 2) and $B_o = 3.4060$ T (point B), respectively. Both spectra were normalized by the ESE signal amplitude without rf irradiation. Experimental conditions are the following: mw frequency, 94.7 GHz; durations of the mw pulses, 60 ns; time interval τ between the first and second mw pulses, 200 ns; time interval T between the second and third mw pulses, 40 μs; rf pulse duration, 35 μs. Dashed trace superimposed on trace A is obtained from trace B by multiplying the latter by 0.28, which is the approximate relative amplitude of the broad background for trace 1 in Figure 2. Trace A-B is the difference between trace A and the dashed trace. This difference represents the spectrum of ^{17}O transitions within $m_S = \pm 1/2$ electron spin manifolds only. Trace S is the result of numerical simulation of ^{17}O Mims ENDOR spectrum for the $m_S = \pm 1/2$ electron spin manifolds. Simulation parameters are the following: $a_{iso} = 0.75$ MHz (the central value); $\Delta a_{iso} = 0.3$ MHz (the width of Gaussian distribution around the central value); $T_\perp = 0.69$ MHz; $e^2Qq/h = 6.5$ MHz; $\eta = 1$; $\varphi_{hq} = 0°$; $\theta_{hq} = 35°$; $\psi_{hq} = 0°$.

the anisotropic hfi, k is the nuclear quadrupole coupling constant ($k = e^2Qq/[4I(2I-1)h]$), and η is the asymmetry parameter of the electric field gradient on the ^{17}O nucleus. X, Y, and Z are the axes of the laboratory coordinate frame, with $\mathbf{B_0}||Z$. X', Y', and Z' are the principal axes of the nqi. The electron spin projection on $\mathbf{B_0}$, m_S ($m_S \equiv \langle S_Z \rangle$), assumes the values from $-7/2$ to 7/2. At magnetic fields used in this work ($B_o \approx 3.4$ T), the electronic Zeeman interaction of Gd^{3+} was about 2 orders of magnitude stronger than the cfi for the studied complexes. Therefore, Hamiltonian eq 1 does not include the average electron spin components $\langle S_X \rangle$ and $\langle S_Y \rangle$ (unlike the spin Hamiltonians employed in our previous studies[16,26] that were performed at the mw X- and K_u-bands).

At $B_o \approx 3.4$ T, ν_O is about -19.6 MHz (it is negative because the g factor of ^{17}O is negative), while the ENDOR features are all located within 3 MHz from $|\nu_O|$. We may therefore conclude that both the hyperfine and quadrupole interactions of ^{17}O are weak compared with the Zeeman interaction, and for the purposes of a qualitative analysis Hamiltonian eq 1 can be considerably simplified:

$$\hat{H} = -\nu_O \hat{I}_Z + m_S(a_{iso} + T_{ZZ})\hat{I}_Z + Q\hat{I}_Z^2 \qquad (2)$$

where $Q = (3/2)k[3b_{Z'Z}^2 - 1 + \eta(b_{X'Z}^2 - b_{Y'Z}^2)]$ and $b_{X'Z}$, $b_{Y'Z}$, and $b_{Z'Z}$ are the direction cosines of the Z axis in the $X'Y'Z'$ frame. The frequencies of ENDOR transitions between the energy levels that correspond to the ^{17}O spin projections m_I and $m_I + 1$ ($m_I \equiv \langle I_Z \rangle$) are then given by

$$\nu_{m_I \leftrightarrow m_I+1} = -\nu_O + m_S(a_{iso} + T_{ZZ}) + Q(2m_I + 1) \qquad (3)$$

Thus, in this approximation, $\nu_{-1/2 \leftrightarrow 1/2}$ is not affected by the nqi at all, while $\nu_{\pm 1/2 \leftrightarrow \pm 3/2}$ and $\nu_{\pm 3/2 \leftrightarrow \pm 5/2}$ are shifted from $\nu_{-1/2 \leftrightarrow 1/2}$ by $\pm 2Q$ and $\pm 4Q$, respectively. These shifts are orientation-dependent, and in an orientationally disordered system the nqi term leads to the broadening and decrease in amplitude of the $\nu_{\pm 1/2 \leftrightarrow \pm 3/2}$ and $\nu_{\pm 3/2 \leftrightarrow \pm 5/2}$ lines. The maximal value of Q is $3k$ (reached for $b_{Z'Z} = 1$), and for the water oxygen with $k \approx 0.16$ MHz (for H_2O ice, $e^2Qq/h \approx 6.5$ MHz[27]) we may expect the shifts of up to $6k \approx 1$ MHz for $\nu_{\pm 1/2 \leftrightarrow \pm 3/2}$ and $12k \approx 2$ MHz for $\nu_{\pm 3/2 \leftrightarrow \pm 5/2}$.

In the difference ENDOR spectrum A-B (Figure 3) the most intense features are the two narrow peaks with the splitting of 1.33 MHz between them. In view of the preceding considerations, these peaks may be safely attributed to the $\nu_{-1/2 \leftrightarrow 1/2}$ frequencies at the perpendicular orientation of the hfi tensor axis relative to $\mathbf{B_0}$. These peaks are denoted as $A_\perp$ to indicate that the splitting between them equals to the hfi constant $A_\perp = a_{iso} + T_\perp$, where $T_\perp$ is the perpendicular component of the anisotropic hfi tensor. The assumption about this tensor being axial, although reasonable at this point, will be verified below by means of numerical simulations. These simulations will also reveal the location of the $A_\parallel$ features in the ENDOR spectrum. On the basis of analysis of eq 3 above, it is anticipated that the two pairs of shoulders with the splittings of about 3.3 and 5.3 MHz are quite likely to be attributed to $\nu_{\pm 1/2 \leftrightarrow \pm 3/2}$ and $\nu_{\pm 3/2 \leftrightarrow \pm 5/2}$, respectively.

The combination of high magnetic field and low temperature used in this work allows us to determine the sign of $A_\perp$ from spectrum B in Figure 3. This spectrum consists of contributions from all EPR transitions other than the $-1/2 \leftrightarrow +1/2$ transition. The relative amplitudes of the $A_\perp$ peaks in spectrum B are determined by the differences in populations of electron spin manifolds with $m_S = -3/2$ and $-1/2$ for one of the peaks and with $m_S = 1/2$ and 3/2 for the other one. At the measurement temperature of about 5.3 K and the Zeeman energy difference of about 4.5 K between the electron spin manifolds with $\Delta m_S = 1$ (corresponds to $B_o \approx 3.4$ T), the amplitude of the $A_\perp$ peak arising from $-3/2 \leftrightarrow -1/2$ electron spin transition should be about 5 times greater than that of the $A_\perp$ peak arising from $1/2 \leftrightarrow 3/2$ electron spin transition. Therefore, the only clearly observable $A_\perp$ peak in spectrum B of Figure 3 is obviously attributed to the $m_S = -1/2$ electron spin manifold. Since this peak is located at a frequency that is less than $|\nu_O|$, it can be immediately concluded that $A_\perp > 0$.

To proceed further, we have to review the characteristic values of the hfi and nqi parameters entering the spin Hamiltonian. The isotropic hfi constants of ^{17}O in Gd^{3+} complexes found by NMR in liquid solutions are on the order of $a_{iso} \approx 0.7$ MHz[13] and correspond to a very small spin density delocalized onto the ^{17}O nucleus ($|\rho_O| \approx 0.004$ as estimated below). With such a small ρ_O, the point dipole approximation employing a Gd−O

distance range of $R_{GdO} \approx 2.37-2.56$ Å [5-9] should provide a fair estimate of the ^{17}O anisotropic hfi: $T_\perp = 0.64-0.80$ MHz. The quadrupole coupling constant for the water molecule in ice or glass is about $k \approx 0.16$ MHz (corresponds to $e^2Qq/h \approx 6.5$ MHz[27]). The nqi asymmetry parameter for the water molecule is expected to be close to unity, $\eta \approx 1$.[27] The orientation of the nqi principal axes frame $X'Y'Z'$ relative to the hfi frame $X_hY_hZ_h$ (Z_h is the main axis) can be defined by the Euler angles φ_{hq}, θ_{hq}, and ψ_{hq}. They are the angles of three consecutive rotations: (1) around Z' by φ_{hq}, (2) around the newly obtained Y' by θ_{hq}, and (3) around the newly obtained Z' by ψ_{hq}. The situation with all of the angles equal to zero corresponds to $X'||X_h$, $Y'||Y_h$, and $Z'||Z_h$. The Z' axis of the nqi tensor is approximately perpendicular to the HOH plane of the water molecule, while the other large axis of the nqi tensor (the Y' axis) is in the HOH plane and perpendicular to the bisector of the HOH angle.[28]

The above parameters were used as an initial approximation in the numerical ENDOR simulations. The simulations were performed using a numerical diagonalization of the full spin Hamiltonian given by eq 1. To reproduce the experimental width of the $A_\perp$ peaks, a Gaussian distribution of a_{iso} with a width of 0.3 MHz was introduced in the simulations. The simulated spectra were in reasonable agreement with the experimental one for the following hfi parameters: $a_{iso} = 0.75 \pm 0.05$ MHz (here and below, a_{iso} indicates the value corresponding to the center of the Gaussian distribution), $T_\perp = 0.69 \mp 0.05$ MHz. Although the above error ranges of the individual hfi parameters are about 0.1 MHz, the sum $a_{iso} + T_\perp$ has to be kept at 1.44 MHz in order to reproduce the experimental $A_\perp$ splitting. This value of $a_{iso} + T_\perp$ is slightly greater than the observable splitting of ~1.33 MHz as a result of the hfi distribution. The two sets of shoulders in the simulated spectra were sensitive to the nqi parameters. The simulations yielded $k = 0.175 \pm 0.012$ MHz ($e^2Qq/h = 7 \pm 0.5$ MHz) and $\eta \geq 0.8$. The calculated and experimental spectra were in reasonable agreement for the values of θ_{hq} from 0° to 90° and $\psi_{hq} \leq 10°$, although the best results were obtained for θ_{hq} in the range from 70° to 80° and $\psi_{hq} \approx 0°$. The third angle, φ_{hq}, is arbitrary because the hfi tensor is nearly axial. An example of a simulated spectrum is shown by trace S in Figure 3.

Figure 4 shows the decomposition of this spectrum into separate nuclear transitions (for $m_S = -1/2$ only) to better illustrate the structure of the simulated as well as the experimental spectra. One can see that the $A_{||}$ features (one of which is shown in the Figure) of the $-1/2 \leftrightarrow +1/2$ transitions in this spectrum are located between the $A_\perp$ ones. The spectral shoulders contain contributions from the $\pm1/2 \leftrightarrow \pm3/2$ and $\pm3/2 \leftrightarrow \pm5/2$ transitions, as anticipated. The transition frequencies of these lines are determined by a combination of the hf and nq interactions (see eq 3). Therefore, the transition frequencies $\nu \approx |\nu_O|$ do not necessarily correspond to $a_{iso} + T_{ZZ} \approx 0$. As a result, these lines are not suppressed in the center of the Mims ENDOR spectrum, in contrast to the situation observed for $I = 1/2$ systems.

The spectrum of contrast agent MS-325 recorded at the EPR position A is presented in Figure 5. There is only one water ligand in MS-325, which results in a significantly lower signal-to-noise ratio than that obtained for the aquo complex. Despite this, one can see that this spectrum is similar in shape to that of the Gd^{3+} aquo ion (the only difference being the narrow matrix line at $\nu = |\nu_O|$ arising from distant ^{17}O nuclei). This indicates that the parameters of the ^{17}O hfi and nqi in these complexes are the same.

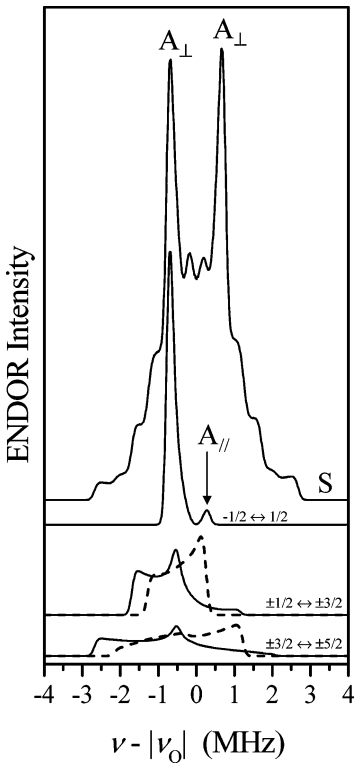

Figure 4. Trace S is the simulated Mims ENDOR spectrum reproduced from Figure 3. Other traces represent the lines of various ^{17}O transitions within the $m_S = -1/2$ electron spin manifold. The m_I values involved in the transitions are shown near the traces. For the two bottom groups of spectra, the solid traces correspond to $m_I < 0$, while the dashed traces correspond to $m_I > 0$. The $A_{||}$ turning point is shown for the $-1/2 \leftrightarrow +1/2$ transition only, the one least affected by the nqi.

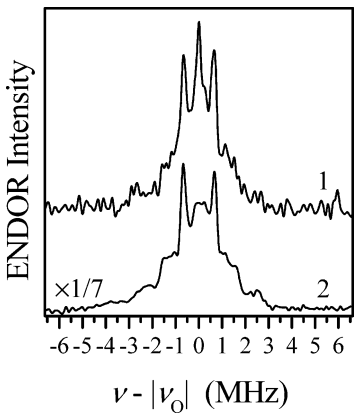

Figure 5. Traces 1 and 2 are, respectively, the ^{17}O Mims ENDOR spectra of MS-325 and Gd aquo complex recorded at $B_o = 3.3966$ T (point A; see Figure 2). The spectra were normalized by the ESE signal amplitude without rf irradiation. In addition, the spectrum of the Gd aquo complex was scaled with the factor of 1/7.

3. Structural Implications of the ENDOR Results. In this section we will discuss the structural implications of the hfi and nqi parameters obtained from the ENDOR spectra. The nqi parameters are close to those known for ice,[27] which may be interpreted as indication that the hybridization of the water oxygen orbitals is close to sp^3. The estimated range of possible nqi orientations (θ_{hq} from 0° to 90° and $\psi_{hq} \approx 0°$) shows that any angle γ between the vector $\mathbf{R_{GdO}}$ and the HOH plane would be in agreement with our experiments as long as the HOH plane is perpendicular to the plane formed by $\mathbf{R_{GdO}}$ and the HOH bisector.

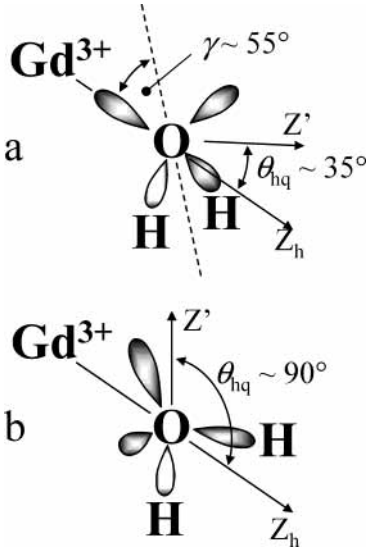

Figure 6. Models of water coordination to Gd^{3+}. In (a) the Gd^{3+} ion is located in the direction pointed by one of the hybrid lone pair orbitals, while in (b) it is located in the HOH plane on the bisector of the HOH angle. Solid arrows show the main axes of the nqi (Z') and hfi (Z_h) tensors. Dashed line in (a) shows the HOH angle bisector that also coincides with the bisector of the angle between the lone pair orbitals. In (b) this bisector coincides with the Z_h axis. Angle γ between this bisector and the Z_h axis is ~55° in (a) and ~0° in (b). Angle θ_{hq} between the Z' and Z_h axes is ~35° in (a) and ~90° in (b).

The anisotropic hfi constant $T_\perp = 0.69 \mp 0.05$ is within the range of 0.64−0.80 MHz evaluated above in a point dipole approximation from the Gd−O distance seen in X-ray studies. This already indicates that the effect of ρ_O on $T_\perp$ is small. A quantitative estimate of this effect can be obtained from analysis of the isotropic hfi constant of ^{17}O. This analysis critically depends on the model employed to describe the coordination of a water molecule to the Gd^{3+} ion, and we will first assume that the coordination involves one of the sp^3 hybrid oxygen orbitals carrying an electron lone pair. In such a configuration, $\gamma \approx 55°$, while $\theta_{hq} = 90° - \gamma \approx 35°$ (see Figure 6a).

The magnitude of a_{iso} is mostly determined by the hybridization of the bonding oxygen orbital and by ρ_O. For a hybrid orbital being a mixture of 2p and 2s orbitals, the isotropic hfi constant is approximately equal to[29]

$$a_{iso} \approx \frac{1}{2S}[a_s c_s + a_p(1 - c_s)]\rho_O \qquad (4)$$

where S is the electron spin of Gd^{3+} ($S = 7/2$), $a_s \approx -5260$ MHz,[30,31] $a_p \approx -120$ MHz,[30,31] and c_s is the s character of the hybrid orbital. For the sp^3 hybrid orbital, $c_s = 1/4$. From $a_{iso} \approx 0.75$ MHz, using eq 4, we can then estimate $\rho_O \approx -4 \times 10^{-3}$.

The anisotropic hfi consists mainly of two contributions: from the spin density on Gd^{3+}, ρ_{Gd}, and the spin density ρ_O:

$$T_\perp \approx -\frac{g\beta g_O \beta_n}{h R_{GdO}{}^3}\rho_{Gd} + \frac{b_p}{2S}(1 - c_s)\rho_O \qquad (5)$$

where g and g_O are, respectively, the electronic and oxygen ^{17}O nuclear g factors, β and β_n are the Bohr magneton and nuclear magneton, and $b_p \approx 170$ MHz.[30,31] The first term in eq 5 describes, in the point dipole approximation, the dipole interaction with the spin density on Gd, while the second term represents the contribution of the spin density delocalized in the bonding orbital of ^{17}O. This expression does not take into account the contributions of the spin density delocalized onto other oxygen ligands because the shortest distance between the oxygens of the water ligands in the Gd^{3+} aquo complex is about 3 Å.

By use of $\rho_O \approx -4 \times 10^{-3}$ estimated from eq 4, the second term in eq 5 is found to be about −0.07 MHz, or about 10% of the value of $T_\perp$ predicted using the point dipole approximation. Neglecting this correction will result in an error in the Gd−O distance estimate of only about 3%. In addition to this simple estimate, one can calculate from eq 5 that the range of $T_\perp$ values obtained in these experiments ($T_\perp = 0.69 \pm 0.05$ MHz) translates into a range of possible distances R_{GdO} between 2.35 and 2.45 Å that is consistent with the range of distances known from X-ray studies.

The contribution of $\rho_O \approx -4 \times 10^{-3}$ to the effective anisotropic hfi constant of the water ligand proton is entirely negligible because the axis of the proton anisotropic hfi tensor associated with ρ_O is at an angle of about 53° to the direction of the main axis of the tensor associated with ρ_{Gd} (assuming for simplicity that ρ_O is located in the center of the oxygen atom). At such relative orientation of the contributing hfi tensors, ρ_O will only lead to a slight rhombicity of the total tensor, without affecting its long axis (effective $T_{||}$) and, correspondingly, the average of its two short axes (effective $T_\perp$). This rhombicity is too small to be detected in an experiment, especially taking into account a rather broad distribution of the anisotropic hfi parameters. Indeed, the estimated difference between the two short axes of the total anisotropic hfi tensor is about 0.1 MHz, while the distribution with of the effective $T_\perp$ value is about 0.4 MHz.[16]

The accuracy of determination of R_{GdO} in this work and R_{GdH} in our previous work[16] is high enough to meaningfully test if these two values are in mutual agreement. Using the structural model for $Gd-OH_2$ coordination formulated above (i.e., that the Gd−O axis coincides with the axis of one of the oxygen lone pair orbitals), we can immediately estimate $R_{GdH} = 2.84-2.93$ Å corresponding to R_{GdO} values of 2.35−2.45 Å. The estimated values of R_{GdH} are significantly shorter than 3.1 ± 0.1 Å found in our previous work[16] (note that the ±0.1 Å is not a measurement error but a characteristic distribution width), and we can conclude that the geometry of Figure 6a may only be responsible for the shortest distance part of the R_{GdH} distribution and has a very low statistical weight.

As an alternative possibility, let us consider the coordination of the water molecule to a metal ion in such a way that the bisector of the lone pairs of the water oxygen is directed toward the ion[32,33] ($\gamma \approx 0°$, $\theta_{hq} \approx 90°$; see Figure 6b). The ion in this case is located in the HOH plane. To estimate ρ_O in this geometry, we can still use eq 4. This ρ_O, however, is a sum of the spin densities delocalized to both lone pair orbitals of the water oxygen ($\rho_O = \rho_{O1} + \rho_{O2}$). The total effect of these spin densities on the oxygen anisotropic hfi will be to make the anisotropic hfi tensor slightly rhombic (with the difference between the two short tensor axes of about 0.14 MHz), without affecting its long axis (effective $T_{||}$) and, correspondingly, the average of its two short axes (effective $T_\perp$). The distance R_{GdO} is therefore accurately estimated directly from the first term in eq 5: $R_{GdO} = 2.41-2.53$ Å. The resulting Gd−H distance for such a coordination geometry is thus $R_{GdH} = 3.08-3.20$ Å. These values are in agreement with the long-distance part of the experimental distance distribution.

To make the agreement complete, we have to note that the assumption about the Gd ion being exactly in the HOH plane certainly represents an idealization. In reality, in glassy samples the angle γ between the Gd−O direction and the HOH plane is

probably distributed in wide limits. An increase in γ will result in a decrease of R_{GdH} estimates, as we have already seen above when we discussed the coordination model of Figure 6a. We suggest therefore that in glassy samples γ is distributed within the limits from 0° (corresponds to Figure 6b) to about 55° (corresponds to Figure 6a), the average value being close to 26° found in neutron diffraction experiments.[8] Such a model brings the R_{GdO} and R_{GdH} values into mutual agreement and allows one to easily explain the distribution of the R_{GdH} values. The corresponding range of the angles θ_{hq} from about 35° to 90° (see Figure 6) does not contradict our experimental results.

Conclusion

In this work we have shown that the essential geometrical parameters of water coordination in Gd^{3+}-based MRI contrast agents (namely, Gd−O and Gd−H distances) can be accurately evaluated from ENDOR spectra of the complexes stabilized in glassy solutions. The high accuracy of these estimates (∼4% for R_{GdO} and ∼3% for the central value of R_{GdH}) becomes possible because for f ions the spin density transfer to the oxygen of the water ligand is extremely small (it is worth noting that for d ions (V^{2+}, Cu^{2+}, Fe^{3+}, Mo^{5+}) the opposite is true, and the structural interpretation of the hfi parameters obtained for d ions is much more involved[34−39]). There are several benefits to the current technique: (1) it does not require single crystals; (2) it does not require high concentrations of the metal complex (1 mM in this work); (3) the complex can be examined in various environments, e.g., in association with plasma proteins.

From the values of R_{GdO} obtained in this work and R_{GdH} obtained earlier,[16] we concluded that the angle between the water molecule plane and the $\mathbf{R_{GdO}}$ vector is likely to be distributed in broad limits, from 0° to about 55°. To test this conclusion, one needs to obtain possibly accurate information about the relative orientation of the ^{17}O nqi and hfi tensors. One-dimensional ENDOR spectra were not sufficiently sensitive to this relative orientation. Our preliminary estimates show, however, that two-dimensional Mims ENDOR[40] or hyperfine correlated ENDOR (HYEND)[41] spectroscopic techniques should be able to distinguish between various structural models. We plan to perform such measurements in the near future.

Acknowledgment. The authors are grateful to Dr. S. Kababya for assistance during experiments. We acknowledge the BSF funding (Grant 2002175) to A.R. and D.G. that allowed us to perform this work.

References and Notes

(1) Caravan, P.; Ellison, J. J.; McMurry, T. J.; Lauffer, R. B. *Chem. Rev.* **1999**, *99*, 9, 2293.
(2) Lauffer, R. B. *Chem. Rev.* **1987**, *87*, 901.
(3) *The Chemistry of Contrast Agents in Medical Magnetic Resonance Imaging*; Merbach, A. E., Toth, E., Eds.; Wiley: New York, 2001.
(4) Clarkson, R. B. In *Topics in Current Chemistry*; Krause, W., Ed.; Springer-Verlag: Berlin, 2002; Vol. 221, p 202.
(5) Steele, M. L.; Wertz, D. L. *J. Am. Chem. Soc.* **1976**, *98*, 4424.
(6) Parker, D.; Puschmann, H.; Batsanov, A. S.; Senanayake, K. *Inorg. Chem.* **2003**, *42*, 8646.
(7) Cossy, C.; Barnes, A.; Enderby, J.; Merbach, A. E. *J. Chem. Phys.* **1989**, *90*, 3254.
(8) Cossy, C.; Helm, L.; Powell, D. H.; Merbach, A. E. *New J. Chem.* **1995**, *19*, 27.
(9) Yamaguchi, T.; Nomura, M.; Wakita, H.; Ohtaki, H. *J. Chem. Phys.* **1988**, *89*, 5153.
(10) Micskei, K.; Helm, L.; Brucher, E.; Merbach, A. E. *Inorg. Chem.* **1993**, *32*, 3844.
(11) Powell, D. H.; Ni Dhubhghaill, O. M.; Pubanz, D.; Helm, L.; Lebedev, Y. S.; Schlaepfer, W.; Merbach, A. E. *J. Am. Chem. Soc.* **1996**, *118*, 9333.
(12) Toth, E.; Adzamli, K.; Periasamy, M. P.; Koenig, S. H.; Merbach, A. E. Adams, M. D. *Magn. Reson. Mater. Phys., Biol. Med.* **1999**, *8*, 163.
(13) Reuben, J.; Fiat, D. *J. Chem. Phys.* **1969**, *51*, 4909.
(14) Aime, S.; Bertini, I.; Luchinat, C. *Coord. Chem. Rev.* **1996**, *150*, 29.
(15) Hoffmann, B. M. *Proc. Natl. Acad. Sci. U.S.A.* **2003**, *100*, 3575.
(16) Astashkin, A. V.; Raitsimring, A. M.; Caravan, P. *J. Phys. Chem. A* **2004**, *108*, 1990.
(17) Ranon, U.; Hyde, J. *Phys. Rev.* **1966**, *141*, 259.
(18) Arieli, D.; Vaughan, D. E. W.; Strohmaier, K. G.; Goldfarb, D. *J. Am. Chem. Soc.* **1999**, *121*, 6028.
(19) Goldfarb, D.; Strohmaier, K. G.; Vaughan, D. E. W.; Thomann, H.; Poluektov, O. G.; Schmidt, J. *J. Am. Chem. Soc.* **1996**, *118*, 4665.
(20) Baes, C. F.; Mesmer, R. E. In *The Hydrolysis of Cations*; Krieger: Malabar, FL, 1986; pp 129−138.
(21) Caravan, P.; Comuzzi, C.; Crooks, W.; McMurry, T. J.; Choppin, G. R.; Woulfe, S. R. *Inorg. Chem.* **2001**, *40*, 2170.
(22) Gromov, I.; Krymov, V.; Manikandan, P.; Arieli, D.; Goldfarb, D. *J. Magn. Reson.* **1999**, *139*, 8.
(23) Mims, W. B. *Proc. R. Soc.* **1965**, *283A*, 452.
(24) Smirnova, T. I.; Smirnov, A. I.; Belford, R. L.; Clarkson, R. B. *Magn. Reson. Mater. Phys., Biol. Med.* **1999**, *8*, 214.
(25) Rast, S.; Borel, A.; Helm, L.; Belorizky, E.; Fries, P. H.; Merbach, A. E. *J. Am. Chem. Soc.* **2001**, *123*, 2637.
(26) Astashkin, A. V.; Raitsimring, A. M. *J. Chem. Phys.* **2002**, *117*, 6121.
(27) Edmonds, D. T.; Zussman, A. *Phys. Lett.* **1972**, *41A*, 167.
(28) Shporer, M.; Achlama, A. M. *J. Chem. Phys.* **1970**, *65*, 3657.
(29) Abragam, A.; Bleaney, B. *Electron Paramagnetic Resonance of Transition Metal Ions*; Clarendon Press: Oxford, U.K., 1970.
(30) Morton, J. R.; Preston, K. F. *J. Magn. Reson.* **1978**, *30*, 577.
(31) Zhidomirov, G. M.; Schastnev, P. V.; Chuvylkin, N. D. *Quantum Chemical Calculations of Magnetic Resonance Parameters*; Nauka: Moscow, 1978.
(32) Chidambaram, R.; Sequeira, A.; Sikka, S. K. *J. Chem. Phys.* **1964**, *41*, 3616.
(33) Sikka, S. K.; Momin, S. N.; Rajagopal, H.; Chidambaram, R. *J. Chem. Phys.* **1968**, *48*, 1883.
(34) Freund, P.; Owen, J.; Hann, B. F. *J. Phys. C: Solid State Phys.* **1973**, *6*, L139.
(35) Freund, P.; Owen, J.; Hann, B. F. *J. Phys. C: Solid State Phys.* **1971**, *4*, L296.
(36) Getz, D.; Silver, B. L. *J. Chem. Phys.* **1974**, *61*, 630.
(37) Greenwood, R. J.; Wilson, G. L.; Pilbrow, J. R.; Wedd, A. G. *J. Am. Chem. Soc.* **1993**, *115*, 5385.
(38) Tan, X.; Bernardo, M.; Thomann, H.; Scholes, C. P. *J. Chem. Phys.* **1993**, *98*, 5147.
(39) Thomann, H.; Bernardo, M.; Kroneck, P. M. H.; Ullrich, V.; Goldfarb, D. *J. Am. Chem. Soc.* **1995**, *117*, 8243.
(40) Liao, P. F.; Hartmann, S. R. *Phys. Rev.* **1973**, *B8*, 69.
(41) Schweiger, A.; Jeschke, G. *Principles of Pulse Electron Paramagnetic Resonance*; Oxford University Press: New York, 2001.